Mixed Formulation for the Natural Element Method in Linear Elasticity

N. Sukumar
Department of Civil Engineering
Northwestern University
Evanston, IL 60208
Dated: July 1998
E-mail: n-sukumar@nwu.edu

Abstract

In this paper, we present a mixed formulation for the Natural Element Method (NEM) in linear elastostatics. In the natural element method, natural neighbor coordinates (Sibson, 1980) are used as the interpolating functions. A displacement-pressure mixed formulation is adopted with displacements interpolated by C^0 natural neighbor shape functions; C^0 and C^{-1} interpolation schemes are considered for the interpolation of the pressure. The mixed C^0–C^{-1} NEM formulation alleviates locking in the near incompressible limit ($\nu \to 0.5$) for the elastostatic boundary value problem. Optimal convergence rates in displacement and energy are obtained for all $\nu \in [0, 0.5)$; however, sub-optimal convergence in the pressure is realized. Results for the cantilever beam in bending, plate with a hole under tension, and rigid inclusion in a plate under uniaxial tension are presented to demonstrate the accuracy and potential of the mixed natural element method.
KEY WORDS: Natural neighbor coordinates, natural element method, mixed formulation, incompressibility

1 Introduction

Variational formulations that are based on Hellinger-Reissner principle and the Hu-Washizu principle (Washizu, 1982) are well-established and widely-used in finite elements. The term mixed methods refers to finite element methods in which two different fields (for eg., displacement and stress or displacement and strain) are approximated as primary variables; in linear elastostatics, mixed methods assume a particular form of the Hellinger-Reissner variational principle. There are significant advantages that accrue when one departs from a displacement-based Galerkin method to one involving a two-field or three-field variational principle. The motivation and

interest in mixed finite element methods stems from quite a few factors: first, in structural analysis the stress tensor $\boldsymbol{\sigma}$ is very often the key field variable of interest, which can be directly obtained from the solution of a mixed analysis; mixed formulations impose less stringent continuity requirements on the trial and test function spaces, and as a result C^0 trial functions suffice for fourth-order problems that are posed in a mixed variational framework; mixed methods facilitate the representation of smoothly varying stress (pressure) fields by using C^0 interpolation for the stresses (pressure); and lastly, the judicious choice of functions spaces for the primary fields in mixed formulations permits robust and accurate solutions of boundary value problems in limiting cases, such as near incompressibility (Poisson locking) in linear elastostatics when the Poisson's ratio $\nu \to 0.5$, and membrane and shear locking in thin beam and plate problems as the thickness $t \to 0$. A caveat to the above optimism is that the choice of function spaces for the primary fields in mixed methods can not be arbitrary; the accuracy and convergence of the method relies on how well the discrete finite-dimensional subspaces approximate their continuous counterparts, and more importantly, if the discrete function spaces satisfy the Ladyzhenskaya-Babuška-Brezzi (LBB) or inf-sup stability condition (Ladyzhenskaya, 1969; Babuška, 1971; Brezzi, 1974).

Locking in finite elements has primarily been approached using modified variational principles, such as assumed strain methods (Simo and Hughes, 1986), assumed stress methods (Pian and Sumihara, 1984), and selective reduced integration procedures (Hughes, 1987). Brezzi and Fortin (1991) present a detailed analysis of these methods which are encompassed within the general framework of mixed methods, and Arnold (1990) presents a lucid account of mixed finite element methods for elliptic problems. It is well known that low-order, h-version finite elements cause Poisson locking as the incompressible limit is approached ($\nu \to 0.5$ or $\lambda \to \infty$). The incompressibility constraint tends to impose far too many constraints in the discrete finite element space, and the trial function space is reduced to nullity leading to the phenomena of mesh locking ($\mathbf{u} \cong 0$). For analytical as well as computational issues related to locking, see Babuška and Suri (1992), Suri (1996), and Chilton and Suri (1997). Mixed methods with displacements and pressure as independent variables, and selective reduced integration procedures have been successful in ameliorating this problem. Malkus and Hughes (1978) have shown the equivalence of mixed finite element methods to selective reduced integration techniques.

The Natural Element Method (NEM) (Braun and Sambridge, 1995) is a novel meshless numerical method for the solution of partial differential equations (PDEs). This method has shown significant promise for second-order and fourth-order elliptic PDEs that arise in solid mechanics (Sukumar, Moran, and Belytschko, 1998; Sukumar and Moran, 1999; Sukumar, 1998). In the natural element method, the trial and test functions are constructed using natural neighbor interpolants (Sibson, 1980; Sibson, 1981). These interpolants are local in character, and are based on the Voronoi tessellation (Preparata and Shamos, 1985) of the set of nodes. As opposed to finite elements, there is no notion of element connectivity in the construction of the NEM

interpolant, and in this context, the numerical implementation is viewed as a meshless or meshfree method.

The scope and application of meshless methods (Belytschko et al., 1996) in mixed formulations has not been explored to any depth so far. In meshless methods, there is greater flexibility than finite elements in the choice and smoothness (C^k, $k > 0$) of trial function spaces. Donning (1997) used the notion of locking-free interpolants that are based on cardinal splines to solve thin as well as thick beam and plate problems using Mindlin-Reissner theory. By judicious choice of local basis functions in the Partition of Unity Method (PUM) (Melenk and Babuška, 1996), Babuška and Zhang (1998) provided a theoretical basis for removing locking in the thin beam limit.

In this paper, we present a mixed displacement-pressure formulation for the natural element method. The outline of this paper is as follows. In the following section, a concise description of natural neighbor interpolation is presented. The displacement and pressure fields used in the mixed NEM formulation are also described. In Section 3, the governing equations for the boundary value problem of linear elastostatics (incompressible and compressible cases) together with the mixed formulation for NEM are described. In Section 4, applications of NEM for the cantilever beam in bending, plate with a hole in tension, and the plate with a circular rigid inclusion under uniaxial tension are presented. Finally, in Section 5, some concluding remarks are mentioned.

2 Natural Neighbor Interpolation

In this section, we briefly touch upon the foundations of Sibson's natural neighbor coordinates (shape functions) that are used in the natural element method. For a more in-depth discussion on the Sibson interpolant and its application to second-order partial differential equations in mechanics, the interested reader can refer to Braun and Sambridge (1995) and Sukumar et al. (1998), and the references therein.

Consider a set of distinct nodes $N = \{n_1, n_2, \ldots, n_M\}$ in $\mathbb{R}^2$. The Voronoi diagram and its dual Delaunay triangulation are one of the most fundamental and useful geometric constructs that define an irregular set of points (nodes). Natural neighbor coordinates, which were introduced by Sibson (1980), are constructed on the basis of the underlying Voronoi tessellation for the nodal set N. The Voronoi diagram (or $1st$-order Voronoi diagram) of the set N is a subdivision of the plane into regions T_I (Voronoi polygons) given by

$$T_I = \{\mathbf{x} \in \mathbb{R}^2 \,:\, d(\mathbf{x}, \mathbf{x}_I) < d(\mathbf{x}, \mathbf{x}_J) \;\forall\; J \neq I\}\,, \tag{2.1}$$

where $d(\mathbf{x}_I, \mathbf{x}_J)$, the Euclidean metric, is the distance between $\mathbf{x}_I$ and $\mathbf{x}_J$.

The Voronoi diagram for a set of seven nodes is shown in Fig. 1a. In Fig. 1b, a point $\mathbf{x}$ is introduced into the Voronoi diagram of the set N. If $\mathbf{x}$ is tessellated along with the nodal set N, then in the newly constructed triangulation based on N and $\mathbf{x}$, the natural neighbors of $\mathbf{x}$ are those nodes which are connected by a Delaunay edge to $\mathbf{x}$. The natural neighbor shape functions of $\mathbf{x}$ with respect to a natural neighbor I

are defined as the ratio of the area of overlap of their Voronoi cells to the total area of the Voronoi cell of $\mathbf{x}$:

$$\phi_I(\mathbf{x}) = \frac{A_I(\mathbf{x})}{A(\mathbf{x})}, \tag{2.2a}$$

$$A(\mathbf{x}) = \sum_{J=1}^{n} A_J(\mathbf{x}), \tag{2.2b}$$

where I ranges from 1 to n in Eq. (2.2a). If the point $\mathbf{x}$ approaches a node ($\mathbf{x} \to \mathbf{x}_I$), $\phi_I(\mathbf{x}) = 1$, and all other shape functions are zero. By this fact, and by construction, the properties of positivity, interpolation, and partition of unity directly follow:

$$0 \leq \phi_I(\mathbf{x}) \leq 1, \quad \phi_I(\mathbf{x}_J) = \delta_{IJ}, \quad \sum_{I=1}^{n} \phi_I(\mathbf{x}) = 1 \ \text{ in } \Omega. \tag{2.3}$$

In addition to the above, natural neighbor shape functions satisfy the local coordinate property (Sibson, 1980), namely

$$\mathbf{x} = \sum_{I=1}^{n} \phi_I(\mathbf{x})\mathbf{x}_I, \tag{2.4}$$

which indicates that the shape functions can exactly reproduce the geometrical coordinates. The above equation in conjunction with the partition of unity property in Eq. (2.3) imply that linear completeness is satisfied by the $C^0(\Omega)$ natural neighbor interpolant.

On using Eq. (2.2a), we can write the first-order derivatives of natural neighbor shape functions as

$$\phi_{I,\alpha}(\mathbf{x}) = \frac{A_{I,\alpha}(\mathbf{x}) - \phi_I(\mathbf{x})A_{,\alpha}(\mathbf{x})}{A(\mathbf{x})}, \quad (\alpha = 1, 2). \tag{2.5}$$

The geometric algorithm proposed by Watson (1992) is used to compute the natural neighbor shape functions and its derivatives.

2.1 Displacement and Pressure Interpolation

We consider the interpolation schemes for the displacements and the pressure in the mixed natural element method. The displacement vectors $\mathbf{u}^h(\mathbf{x}) : \ \Omega \subset \mathbb{R}^2 \to \mathbb{R}^2$ are interpolated using natural neighbor shape functions, and can be written in the form:

$$\mathbf{u}^h(\mathbf{x}) = \sum_{I=1}^{n} \phi_I(\mathbf{x})\mathbf{u}_I, \tag{2.6}$$

where $\mathbf{u}_I$ ($I = 1, 2, \ldots, n$) are the vectors of nodal displacements at the n natural neighbors, and $\phi_I(\mathbf{x})$ are the shape functions associated with each node.

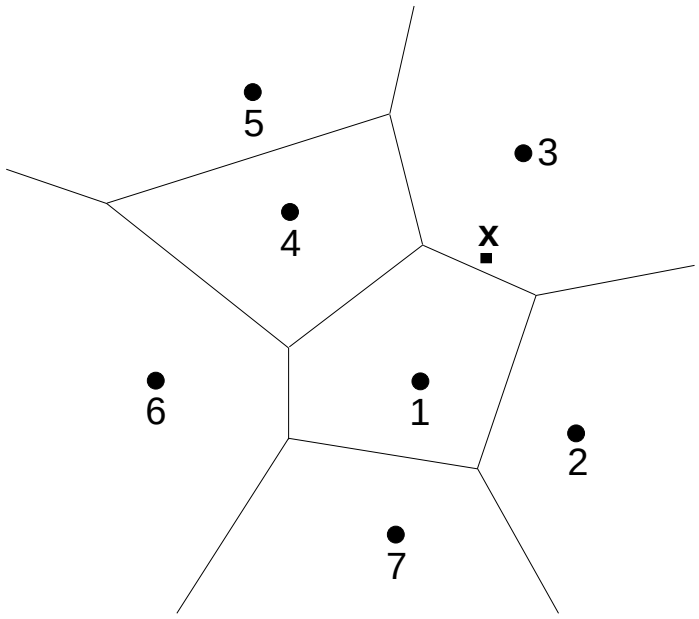

(a)

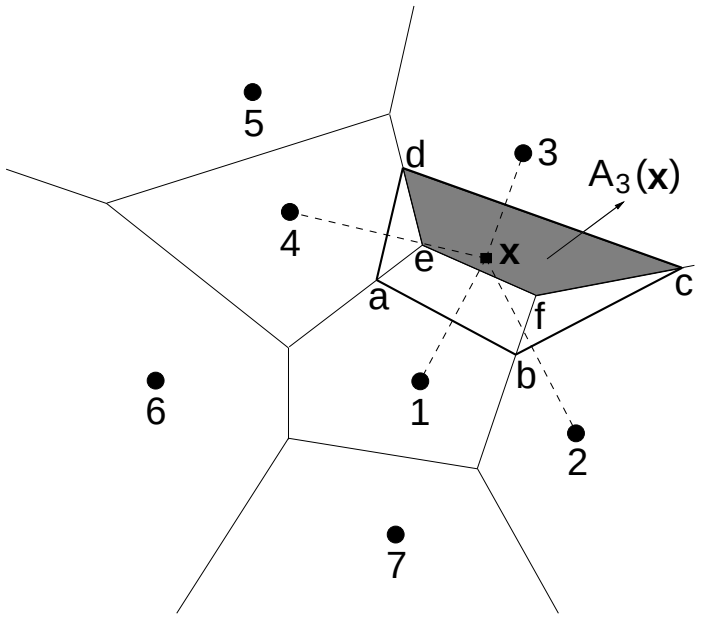

(b)

Figure 1: Construction of natural neighbor coordinates. (a) Original Voronoi diagram and $\mathbf{x}$, and (b) $1st$-order and $2nd$-order Voronoi cells about $\mathbf{x}$.

The pressure field is interpolated by an interpolation scheme akin to Eq. (2.6):

$$p^h(\mathbf{x}) = \sum_{I=1}^{n} \psi_I(\mathbf{x})\bar{p}_I, \tag{2.7}$$

where $\psi_I(\mathbf{x})$ is the shape function associated with node I and $\bar{p}_I$ are the nodal pressures. We consider $\psi_I(\mathbf{x})$ to be of the general form

$$\psi_I(\mathbf{x}) = \frac{\big(\phi_I(\mathbf{x})\big)^k}{\sum_J \big(\phi_J(\mathbf{x})\big)^k}, \tag{2.8}$$

where k is a non-negative integer. The case $k = 1$ reduces to natural neighbor interpolation, and all other k render shape functions that form a partition of unity, with the resulting interpolant satisfying only constant completeness. For $k > 1$, numerical studies show that severe Poisson locking results; the cases $k = 0$ and $k = 1$ alleviated locking in the near incompressible limit and hence merit investigation. These two cases are considered for the interpolation of the pressure field, and Eq. (2.7) takes the specific forms:

$$p^h(\mathbf{x}) = \sum_{I=1}^{n} \frac{1}{n}\bar{p}_I, \tag{2.9a}$$

$$p^h(\mathbf{x}) = \sum_{I=1}^{n} \phi_I(\mathbf{x})\bar{p}_I. \tag{2.9b}$$

The shape functions $\psi_I(\mathbf{x})$ for $k = 0$ that are used to interpolate the pressure need some elaboration. Since the shape functions $\phi_I(\mathbf{x})$ have compact support (Farin, 1990), Eqs. (2.6) and (2.7) are local interpolation schemes. The support of the shape function $\phi_I(\mathbf{x})$ is the intersection of the convex hull CH(N) with the union of all Delaunay circumcircles that pass through node I. In Fig. 2a, a unit square is discretized by 25 (5×5) equi-spaced nodes. The support for node A is illustrated in Fig. 2b—node A is located at the center where $\phi_A(\mathbf{x}_A)$ takes on the value of unity. On the basis of Eq. (2.9a) in conjunction with the above discussion on the support of the C^0 natural neighbor shape functions, we note that the shape functions $\psi_I(\mathbf{x}) = 1/n$ are C^{-1}. Since the shape function $\psi_I(\mathbf{x}) = 1/n$ is the inverse of the number of natural neighbors for a point $\mathbf{x}$, the above inference is readily observed. An alternate C^{-1} pressure interpolant can be constructed using the well-known concept of nearest neighbors in computational geometry (Preparata and Shamos, 1985). This leads to the interpolation scheme known as nearest neighbor interpolation. In this approach, if $\mathbf{x} \in T_I$, where T_I is the Voronoi polygon of node I, then we assign the nodal pressure $\bar{p}_I$ to $p(\mathbf{x})$. In essence, the pressure field is assumed to be a constant over the Voronoi polygon T_I. In the context of natural neighbor interpolation, if $\phi_I = \|\boldsymbol{\phi}\|_\infty$, then $\psi_I(\mathbf{x}) = 1$ and $\psi_J(\mathbf{x}) = 0 \;\forall\; J \neq I$, and therefore

$$p(\mathbf{x}) = \bar{p}_I \quad \text{if } \mathbf{x} \in T_I. \tag{2.10}$$

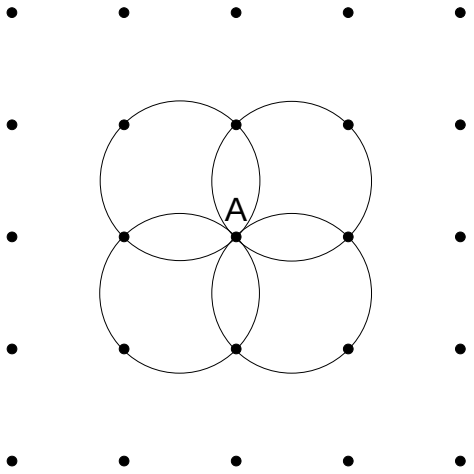

(a)

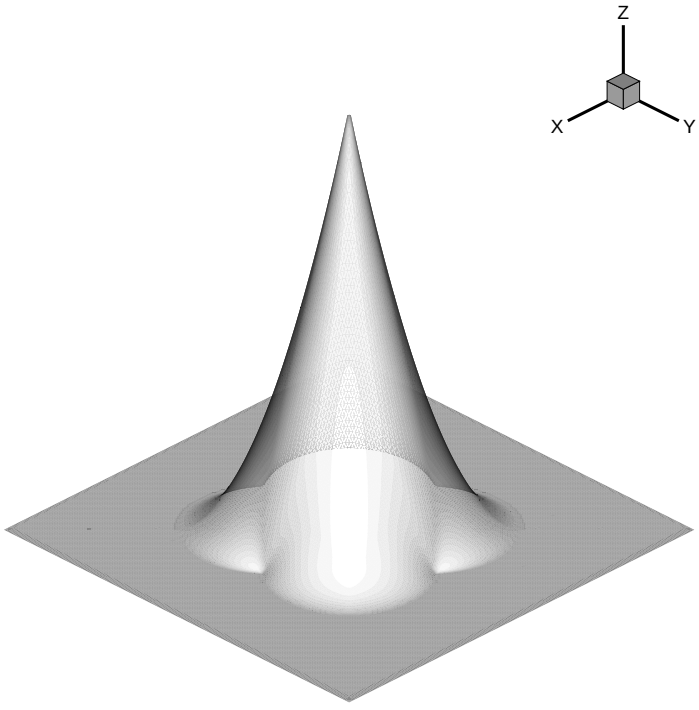

(b)

Figure 2: Support for NEM shape function. (a) Nodal grid, and (b) Shape function $\phi_A(\mathbf{x})$ for node A.

On the boundary of the convex hull, the interpolant is strictly linear (Farin, 1990). By virtue of the interpolation property and the above fact, it follows that essential boundary conditions can be directly imposed on the nodes that lie on the displacement (essential) boundary Γ_u.

3 Governing Equations and Mixed Formulation

3.1 Strong Form

Consider an open bounded domain $\Omega \subset \mathbb{R}^2$ with boundary Γ. Let $\mathbf{n}$ be the unit normal vector to Γ; the closure of Ω is denoted by $\bar{\Omega} = \Omega \cup \Gamma$. We consider the governing equations for two-dimensional small displacement elastostatics, with validity for both compressible and incompressible material behavior. Let the prescribed values of tractions on the traction boundary Γ_t be $\bar{\mathbf{t}}$ and that on the essential boundary Γ_u be $\bar{\mathbf{u}}$ ($\Gamma = \Gamma_u \cup \Gamma_t$). We let $\boldsymbol{\sigma}$ be the Cauchy stress for a kinematically admissible displacement field $\mathbf{u}$, and $\mathbf{b}$ be the body force per unit volume. The strong form for the elastostatic boundary value problem is given by (Hughes, 1987)

$$\text{Given } \mathbf{b} : \Omega \times \Omega \to \mathbb{R}^2,\ \bar{\mathbf{u}} : \Gamma_u \times \Gamma_u \to \mathbb{R}^2,\ \text{and } \bar{\mathbf{t}} : \Gamma_t \times \Gamma_t \to \mathbb{R}^2$$

$$\text{Find } \mathbf{u} : \bar{\Omega} \times \bar{\Omega} \to \mathbb{R}^2,\ p : \bar{\Omega} \to \mathbb{R} \text{ such that}$$

$$\boldsymbol{\nabla} \cdot \boldsymbol{\sigma} + \mathbf{b} = 0 \quad \text{in } \Omega, \tag{3.1a}$$

$$\boldsymbol{\nabla} \cdot \mathbf{u} + \frac{p}{\lambda} = 0 \quad \text{in } \Omega, \tag{3.1b}$$

$$\mathbf{u} = \bar{\mathbf{u}} \quad \text{on } \Gamma_u, \tag{3.1c}$$

$$\boldsymbol{\sigma} \cdot \mathbf{n} = \bar{\mathbf{t}} \quad \text{on } \Gamma_t, \tag{3.1d}$$

where the Cauchy stress tensor $\boldsymbol{\sigma}$ is related to the small strain tensor $\boldsymbol{\varepsilon}$ and the pressure parameter p (hydrostatic pressure if $\nu = 0.5$) for an isotropic linear elastic material through the constitutive relation:

$$\sigma_{ij} = -p\delta_{ij} + \bar{C}_{ijkl}\varepsilon_{kl}, \tag{3.1e}$$

$$\bar{C}_{ijkl} = \mu(\delta_{ik}\delta_{jl} + \delta_{il}\delta_{jk}). \tag{3.1f}$$

In Eq. (3.1), λ and μ are Lamé parameters which for plane strain are defined as

$$\lambda = \frac{\nu E}{(1+\nu)(1-2\nu)}, \quad \mu = \frac{E}{2(1+\nu)}, \tag{3.2}$$

where ν is the Poisson's ratio. The kinematic relation between the small strain tensor $\boldsymbol{\varepsilon}$ and the displacement vector $\mathbf{u}$ is

$$\boldsymbol{\varepsilon} = \frac{1}{2}\left(\boldsymbol{\nabla}\mathbf{u} + (\boldsymbol{\nabla}\mathbf{u})^T\right). \tag{3.3}$$

3.2 Weak Formulation

We first define the trial and test spaces for the displacements and the pressure. Following Hughes (1987), we let

$$\mathbf{u} \in \mathbf{V} = \left(H^1(\Omega)\right)^2 \quad \text{(displacement trial solution space)}, \tag{3.4a}$$

$$\mathbf{v} \in \mathbf{V}_0 = \left(H^1_0(\Omega)\right)^2 \quad \text{(displacement test function space)}, \tag{3.4b}$$

$$p,\, q \in P = L^2(\Omega) \quad \text{(space of pressures—trial and test functions)}, \tag{3.4c}$$

where $H^1(\Omega)$ is the Sobolev space of functions with square-integrable first derivatives in Ω, and $H^1_0(\Omega)$ is the Sobolev space of functions with square-integrable first derivatives in Ω and vanishing values on the essential boundary Γ_u. The weak form of Eq. (3.1) in Hermann variational form is posed as (Hermann, 1965; Hughes, 1987):

$$\begin{aligned} &\text{Find } (\mathbf{u}, p) \in \mathbf{V} \times P \text{ such that} \\ &\bar{a}(\mathbf{u}, \mathbf{v}) + b(\mathbf{v}, p) = \langle \mathbf{b}, \mathbf{v} \rangle + \langle \bar{\mathbf{t}}, \mathbf{v} \rangle \quad \forall\, \mathbf{v} \in \mathbf{V}_0, \end{aligned} \tag{3.5a}$$

$$b(\mathbf{u}, q) - \frac{1}{\lambda}(p, q) = 0 \quad \forall\, q \in P, \tag{3.5b}$$

where

$$\bar{a}(\mathbf{u}, \mathbf{v}) = 2\mu \int_\Omega \varepsilon_{ij}(\mathbf{u}) \varepsilon_{ij}(\mathbf{v})\, d\Omega, \tag{3.5c}$$

$$b(\mathbf{v}, p) = -\int_\Omega p \boldsymbol{\nabla} \cdot \mathbf{v}\, d\Omega. \tag{3.5d}$$

In a displacement-pressure mixed formulation for linear elasticity, the bilinear form $\bar{a}(\mathbf{u}, \mathbf{v}) : \mathbf{V} \times \mathbf{V}_0 \to \mathbb{R}$ is symmetric, bounded, and positive definite. Hence, for the displacement-pressure pair $(\mathbf{u}, p)$ to be the unique solution to the system in Eq. (3.5), the bilinear form $b(\mathbf{v}, p) : \mathbf{V}_0 \times P \to \mathbb{R}$ must satisfy the LBB stability condition (Brezzi and Fortin, 1991):

$$\inf_{p \in P} \sup_{\mathbf{v} \in \mathbf{V}_0} \frac{|b(\mathbf{v}, p)|}{||\mathbf{v}||\mathbf{v}||p||_P} \geq \beta > 0, \tag{3.6}$$

where β is a constant.

In the numerical implementation, finite-dimensional subspaces are used as the trial and test spaces for the displacements and pressure. Let $\mathbf{V}^h \subset \mathbf{V}$ and $\mathbf{V}^h_0 \subset \mathbf{V}_0$ be the trial and test spaces for the displacements, and $P^h \subset P$ be the trial and test space for the pressure. The weak form for NEM can be written as

$$\begin{aligned} &\text{Find } (\mathbf{u}^h, p^h) \in \mathbf{V}^h \times P^h \text{ such that} \\ &\bar{a}(\mathbf{u}^h, \mathbf{v}^h) + b(\mathbf{v}^h, p^h) = \langle \mathbf{b}, \mathbf{v}^h \rangle + \langle \bar{\mathbf{t}}, \mathbf{v}^h \rangle \quad \forall\, \mathbf{v}^h \in \mathbf{V}^h_0, \end{aligned} \tag{3.7a}$$

$$b(\mathbf{u}^h, q^h) - \frac{1}{\lambda}(p^h, q^h) = 0 \quad \forall\, q^h \in P^h. \tag{3.7b}$$

The LBB stability condition for the discrete problem is similar to Eq. (3.6), with the trial and test functions in the continuous space being replaced by their discrete counterparts.

3.3 Discrete System for NEM

Consider the numerical implementation for the mixed natural element method. In a Galerkin procedure, the displacement trial and test functions are interpolated using the same set of shape functions and likewise for the pressure trial and test functions. The trial and test functions are:

$$\mathbf{u}^h(\mathbf{x}) = \sum_{I=1}^{n} \phi_I(\mathbf{x})\mathbf{u}_I, \quad \mathbf{v}^h(\mathbf{x}) = \sum_{I=1}^{n} \phi_I(\mathbf{x})\mathbf{v}_I, \tag{3.8a}$$

$$p^h(\mathbf{x}) = \sum_{I=1}^{n} \psi_I(\mathbf{x})\bar{p}_I, \quad q^h(\mathbf{x}) = \sum_{I=1}^{n} \psi_I(\mathbf{x})\bar{q}_I. \tag{3.8b}$$

The strain-displacement relation for the displacement trial function can be written as

$$\boldsymbol{\varepsilon}^h(\mathbf{x}) = \sum_{I=1}^{n} \mathbf{B}_I \mathbf{u}_I, \tag{3.9}$$

where

$$\mathbf{B}_I = \begin{bmatrix} \phi_{I,1}(\mathbf{x}) & 0 \\ 0 & \phi_{I,2}(\mathbf{x}) \\ \phi_{I,2}(\mathbf{x}) & \phi_{I,1}(\mathbf{x}) \end{bmatrix}. \tag{3.10}$$

The divergence of the displacement trial solution is given by

$$\boldsymbol{\nabla} \cdot \mathbf{u}^h(\mathbf{x}) = \sum_{I=1}^{n} \tilde{\mathbf{B}}_I \mathbf{u}_I, \tag{3.11}$$

where

$$\tilde{\mathbf{B}}_I = \begin{bmatrix} \phi_{I,1}(\mathbf{x}) & \phi_{I,2}(\mathbf{x}) \end{bmatrix}. \tag{3.12}$$

On substituting the displacement and pressure trial and test functions in Eq. (3.7) and using the arbitrariness of displacement and pressure nodal variations, the following discrete system of linear equations is obtained (Hughes, 1987):

$$\begin{bmatrix} \bar{\mathbf{K}} & \mathbf{G} \\ \mathbf{G}^T & \mathbf{M} \end{bmatrix} \begin{Bmatrix} \mathbf{d} \\ \mathbf{p} \end{Bmatrix} = \begin{Bmatrix} \mathbf{f} \\ \mathbf{0} \end{Bmatrix}, \tag{3.13}$$

where

$$\bar{\mathbf{K}}_{IJ} = \int_{\Omega^h} \mathbf{B}_I^T \bar{\mathbf{C}} \mathbf{B}_J \, d\Omega, \tag{3.14a}$$

$$\mathbf{G}_{IJ} = -\int_{\Omega^h} \tilde{\mathbf{B}}_I^T \psi_J \, d\Omega, \tag{3.14b}$$

$$\mathbf{M}_{IJ} = -\frac{1}{\lambda} \int_{\Omega^h} \psi_I \psi_J \, d\Omega, \tag{3.14c}$$

$$\mathbf{f}_I = \int_{\Omega^h} \phi_I \mathbf{b} \, d\Omega + \int_{\Gamma_t^h} \phi_I \bar{\mathbf{t}} \, d\Gamma. \tag{3.14d}$$

In the above equations, $\mathbf{d}$ is the vector of nodal displacements and $\mathbf{p}$ is the vector of nodal pressures. The matrix $\bar{\mathbf{K}}$ is symmetric and positive definite, and the matrix $\mathbf{M}$ is symmetric and negative definite ($\mathbf{M} = \mathbf{0}$ when $\nu = 0.5$). The matrix $\mathbf{G}$ corresponds to the discrete gradient operator, and $\mathbf{G}^T$ to the discrete divergence operator.

4 Numerical Results and Discussions

The application of the mixed natural element method to problems in small displacement compressible as well as near incompressible two-dimensional elastostatics, in the absence of body forces, is presented. In the computations, numerical integration is carried out using symmetric quadrature rules for a triangle (Dunavant, 1985). Three point quadrature rule is used in the numerical integration of the weak form; the error norm computations are carried out using 25 point quadrature rule in each triangle.

4.1 Cantilever Beam

In Fig. 3, a cantilever beam subjected to a parabolic end load is illustrated. The beam has length L, height D, and unit thickness. The displacement vector solution is given by (Timoshenko and Goodier, 1970)

$$u_1(x_1, x_2) = \frac{-P x_2}{6\bar{E}I} \left[(6L - 3x_1)x_1 + (2 + \bar{\nu})x_2^2 - \frac{3D^2}{2}(1 + \bar{\nu}) \right], \tag{4.1a}$$

$$u_2(x_1, x_2) = \frac{P}{6\bar{E}I} \left[3\bar{\nu} x_2^2 (L - x_1) + (3L - x_1)x_1^2 \right], \tag{4.1b}$$

where

$$\bar{E} = \begin{cases} E & \text{(plane stress)}, \\ \dfrac{E}{1 - \nu^2} & \text{(plane strain)}, \end{cases} \tag{4.2a}$$

$$\bar{\nu} = \begin{cases} \nu & \text{(plane stress)}, \\ \dfrac{\nu}{1 - \nu} & \text{(plane strain)}. \end{cases} \tag{4.2b}$$

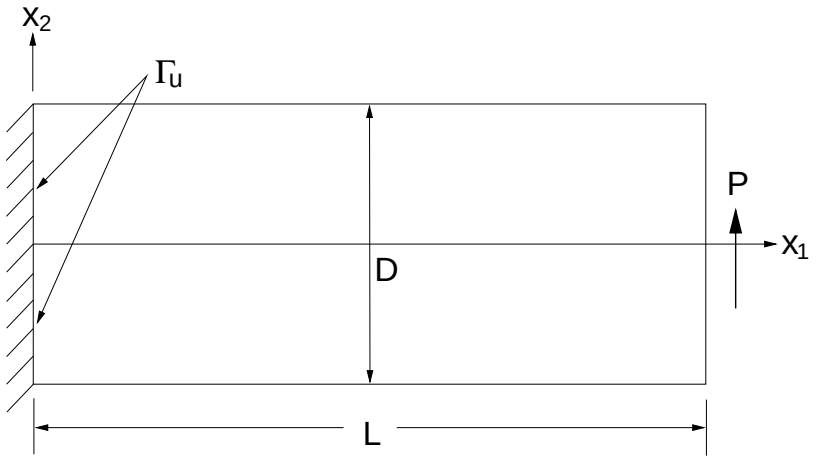

Figure 3: Cantilever beam model.

The stresses are given by

$$\sigma_{11}(x_1, x_2) = \frac{-P(L - x_1)x_2}{I}, \tag{4.3a}$$

$$\sigma_{22}(x_1, x_2) = 0, \tag{4.3b}$$

$$\sigma_{12}(x_1, x_2) = \frac{P}{2I}(\frac{D^2}{4} - x_2^2), \tag{4.3c}$$

where I is the moment of inertia, which for a beam with rectangular cross-section and unit thickness is:

$$I = \frac{D^3}{12}. \tag{4.3d}$$

In the numerical model, the analytical displacement solution from Eq. (4.1) is prescribed on the boundary Γ_u: $x_1 = 0$, $-D/2 \leq x_2 \leq D/2$ (Fig. 3). On the remaining boundaries, exact tractions are specified. The following parameters are used in the numerical computations: $D = 1$ in., $L = 4$ in., $P = -1000$ lb, $E = 3 \times 10^7$ psi, and plane strain conditions are assumed.

The mixed natural element displacement-pressure formulation is applied to both the compressible and near incompressible cases. The numerical computations are carried out using four different nodal discretizations, namely 85 nodes, 297 nodes, 1105 nodes, and 1701 nodes. Equal nodal spacing in the x_1- and x_2-direction is used in each of the above grids. A sample nodal discretization (85 nodes) is shown in Fig. 4. In Table 1, the normalized end displacement $\left(u_2^h(4,0)/u_2(4,0)\right)$ is presented for varying Poisson's ratio using FEM, C^0 NEM, and the mixed formulation. The results presented in Table 1 are for the nodal discretization shown in Fig. 4. Bilinear quadrilateral elements with 3×3 Gauss quadrature are used in the finite element computations, and three point symmetric quadrature rule over triangles is used in

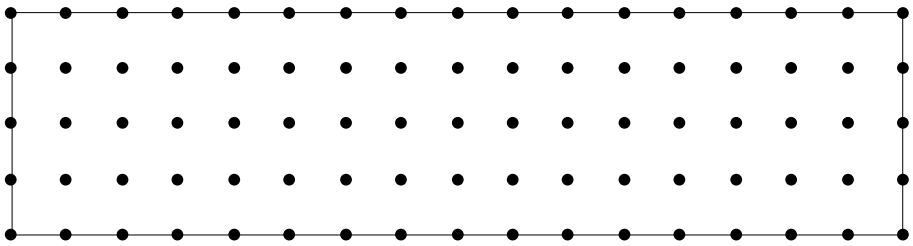

Figure 4: Nodal discretization for cantilever beam model (85 nodes).

the NEM computations. Clearly, severe locking is observed for both, FEM and NEM as $\nu \to 0.5$; the mixed C^0–C^0 method does lock to some degree, but the mixed C^0–C^{-1} method alleviates locking as the incompressible limit is approached. The results for the mixed C^0–C^{-1} formulation are accurate for the entire range of values of ν. A convergence study for the cantilever beam problem is carried out. We define the

Table 1: Normalized end displacement for the cantilever beam problem.

ν	FEM	NEM		
	(3×3)	C^0	Mixed (C^0–C^0)	Mixed (C^0–C^{-1})
0.3	0.9651	0.9692	0.9739	0.9903
0.4	0.9373	0.9436	0.9676	0.9924
0.4999	0.1873	0.1950	0.9495	0.9901
0.4999999	0.1775	0.2103	0.9490	0.9903

$L^2(\Omega)$ and energy error norms used in the analysis as:

$$\|\mathbf{u} - \mathbf{u}^h\|_{L^2(\Omega)} = \Big(\big(\mathbf{u} - \mathbf{u}^h, \mathbf{u} - \mathbf{u}^h\big) \Big)^{1/2}, \tag{4.4a}$$

$$\|\mathbf{u} - \mathbf{u}^h\|_{E(\Omega)} = \left(\frac{1}{2} a\big(\mathbf{u} - \mathbf{u}^h, \mathbf{u} - \mathbf{u}^h\big) \right)^{1/2}, \tag{4.4b}$$

where

$$a(\mathbf{u},\mathbf{u}) = 2\mu\big(\boldsymbol{\varepsilon}(\mathbf{u}),\boldsymbol{\varepsilon}(\mathbf{u})\big) + \lambda^{-1}(p,p). \tag{4.4c}$$

In Figures 5 and 6, the relative displacement and energy error norms are plotted against the nodal spacing h on a log-log plot. Results are presented for the mixed C^0–C^0 displacement-pressure and C^0–C^{-1} displacement-pressure formulations. The error norm computations are carried out for three different values of the Poisson's ratio: $\nu = 0.3$, $\nu = 0.4$, and $\nu = 0.4999$ (near incompressibility). The rate of convergence is denoted by the value of R. The results indicate that optimal convergence in displacement and energy is attained for all three values of ν. The absolute accuracy of the C^0–C^{-1} formulation is better than that obtained for the C^0–C^0 formulation.

The pressure computations are carried out along the mid-section of the beam using the mixed C^0–C^0 and C^0–C^{-1} methods. The results are computed at 100 equi-distant points between $y = -0.5$ in. and $y = 0.5$ in. In Fig. 7, the variation of the pressure parameter p for the 85 node grid is shown for the compressible case ($\nu = 0.3$). The pressure parameter p is given by

$$p = \frac{-\sigma_{kk} + 2\mu\varepsilon_{kk}}{3}, \tag{4.5}$$

and hence in the incompressible limit (div $\mathbf{u} = \varepsilon_{kk} = 0$), p is the hydrostatic pressure. In Fig. 8, the hydrostatic pressure is plotted for the near incompressible case (85 and 1701 nodal grids). The pressure oscillation for the C^0–C^0 method are fairly pronounced, while the results for the C^0–C^{-1} method are less oscillatory.

4.2 Infinite Plate with a Circular Hole

In order to test the accuracy of the mixed formulation in near incompressible elasticity, it is imperative that we also study its performance for curvilinear domains which require non-uniform nodal discretizations. To this end, we study two benchmark problems. First, we consider the problem of an infinite plate with a traction free circular hole under unidirectional tension along the x_1-direction (Fig. 9). The exact solution to this problem is given in Timoshenko and Goodier (1970) as well as Szabó and Babuška (1991). The domain $ABCDE$ shown in Fig. 9 is modeled with the exact tractions imposed along BC and CD. Due to symmetry, the essential boundary conditions are: $u_2 = 0$ along AB, and $u_1 = 0$ along DE. In polar coordinates (r,θ), the exact stress distribution for $\sigma_0 = 1$ psi is given by

$$\sigma_{11}(r,\theta) = 1 - \frac{a^2}{r^2}\left(\frac{3}{2}\cos 2\theta + \cos 4\theta\right) + \frac{3}{2}\frac{a^4}{r^4}\cos 4\theta, \tag{4.6a}$$

$$\sigma_{22}(r,\theta) = -\frac{a^2}{r^2}\left(\frac{1}{2}\cos 2\theta - \cos 4\theta\right) - \frac{3}{2}\frac{a^4}{r^4}\cos 4\theta, \tag{4.6b}$$

$$\sigma_{12}(r,\theta) = -\frac{a^2}{r^2}\left(\frac{1}{2}\sin 2\theta + \sin 4\theta\right) + \frac{3}{2}\frac{a^4}{r^4}\sin 4\theta, \tag{4.6c}$$

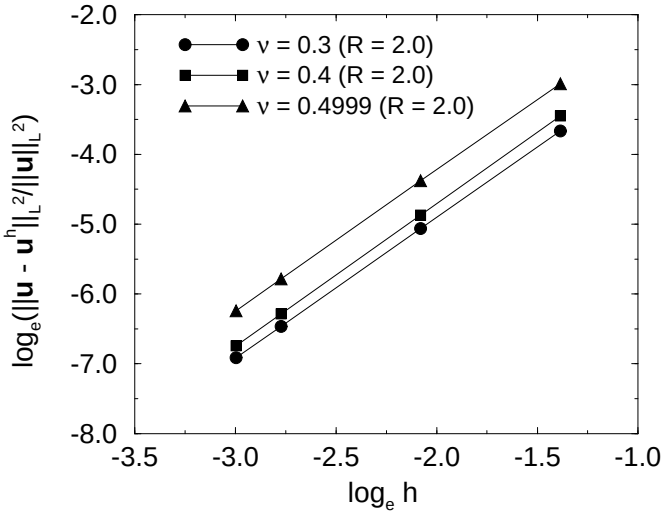

(a)

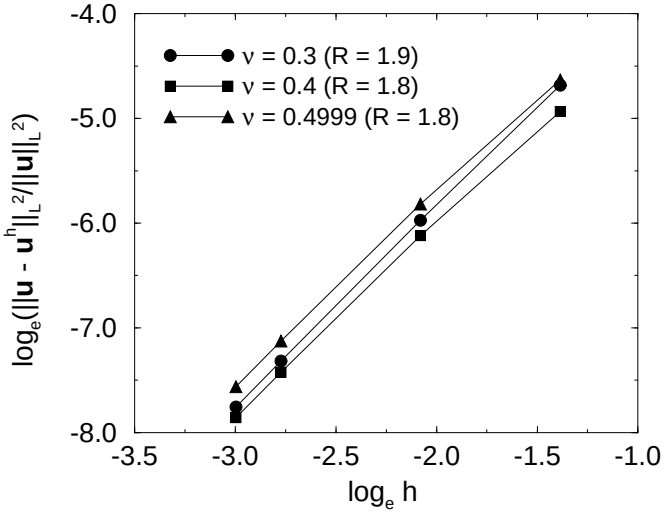

(b)

Figure 5: Rate of convergence in displacement for the cantilever beam problem. (a) C^0–C^0 method, and (b) C^0–C^{-1} method.

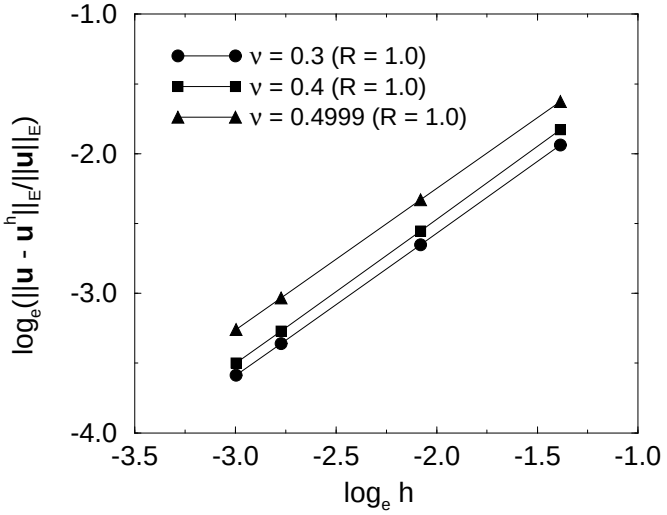

(a)

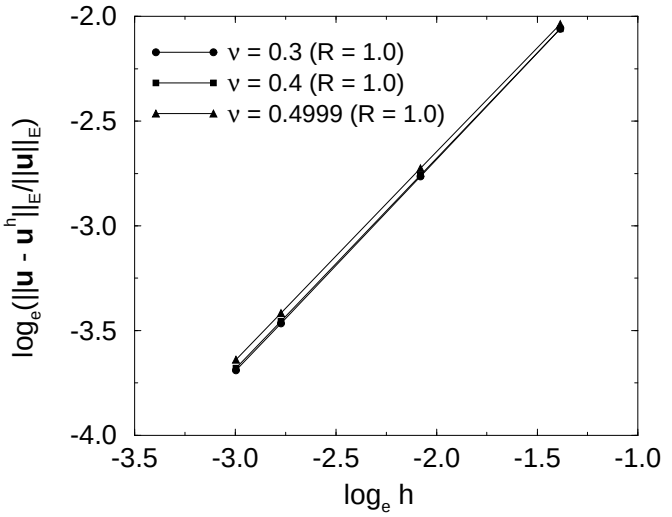

(b)

Figure 6: Rate of convergence in energy for the cantilever beam problem. (a) C^0–C^0 method, and (b) C^0–C^{-1} method.

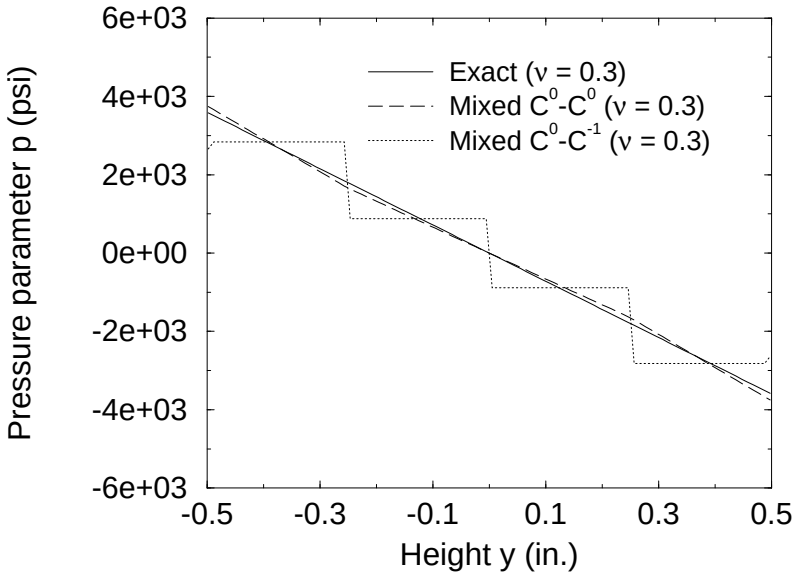

Figure 7: Variation of the pressure parameter p for the beam model.

where a is the radius of the circular hole. The displacement components (rigid-body displacement and rotation set to zero) are:

$$u_1(r,\theta) = \frac{a}{8\mu}\left[\frac{r}{a}(\kappa+1)\cos\theta + 2\frac{a}{r}((1+\kappa)\cos\theta + \cos 3\theta) - 2\frac{a^3}{r^3}\cos 3\theta\right], \qquad (4.7a)$$

$$u_2(r,\theta) = \frac{a}{8\mu}\left[\frac{r}{a}(\kappa-3)\sin\theta + 2\frac{a}{r}((1-\kappa)\sin\theta + \sin 3\theta) - 2\frac{a^3}{r^3}\sin 3\theta\right], \qquad (4.7b)$$

where μ is the shear modulus and κ (Kolosov constant) is defined as

$$\kappa = \begin{cases} 3-4\nu & \text{(plane strain)}, \\ \dfrac{3-\nu}{1+\nu} & \text{(plane stress)}. \end{cases} \qquad (4.8)$$

In the numerical computations, $a = 1$ in., $L = 5$ in., and plane strain conditions are assumed. The nodal discretizations used in the computations are shown in Fig. 10. The mixed natural element displacement-pressure formulation is applied to both the compressible and near incompressible cases. A convergence study is carried out using four different nodal discretizations (Fig. 10). The $L^2(\Omega)$ and energy error norms used in the computations are defined in Eq. (4.4). In Figures 11 and 12, the relative displacement and energy error norms are plotted against the square root of the number of nodes on a log-log plot. Results are presented for the mixed C^0–C^0 displacement-pressure and C^0–C^{-1} displacement-pressure formulations. The error norm computations are carried out for three different values of the Poisson's ratio: $\nu = 0.3$, $\nu = 0.4$, and $\nu = 0.4999$ (near incompressibility). The convergence rates

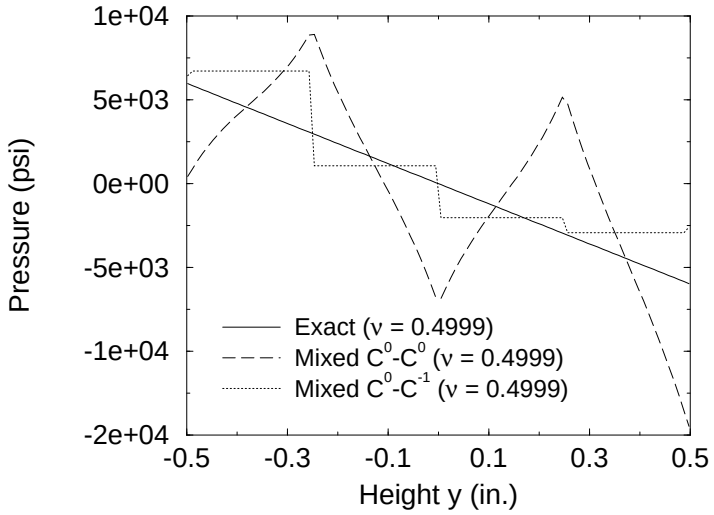

(a)

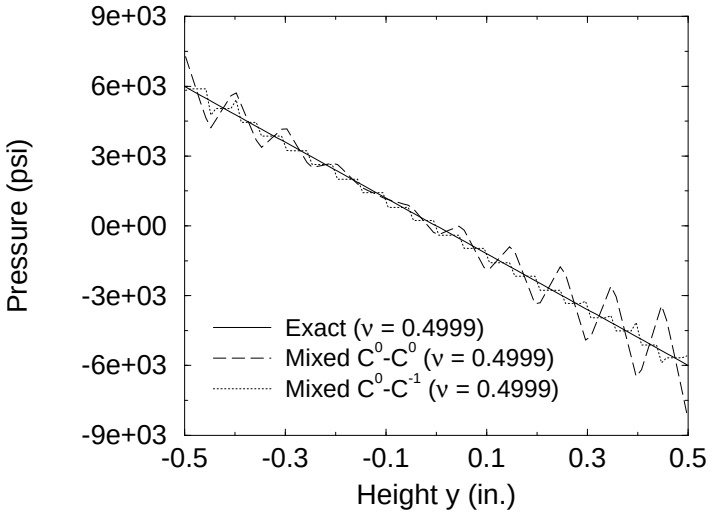

(b)

Figure 8: Variation of hydrostatic pressure for the beam model. (a) 85 nodes, and (b) 1701 nodes.

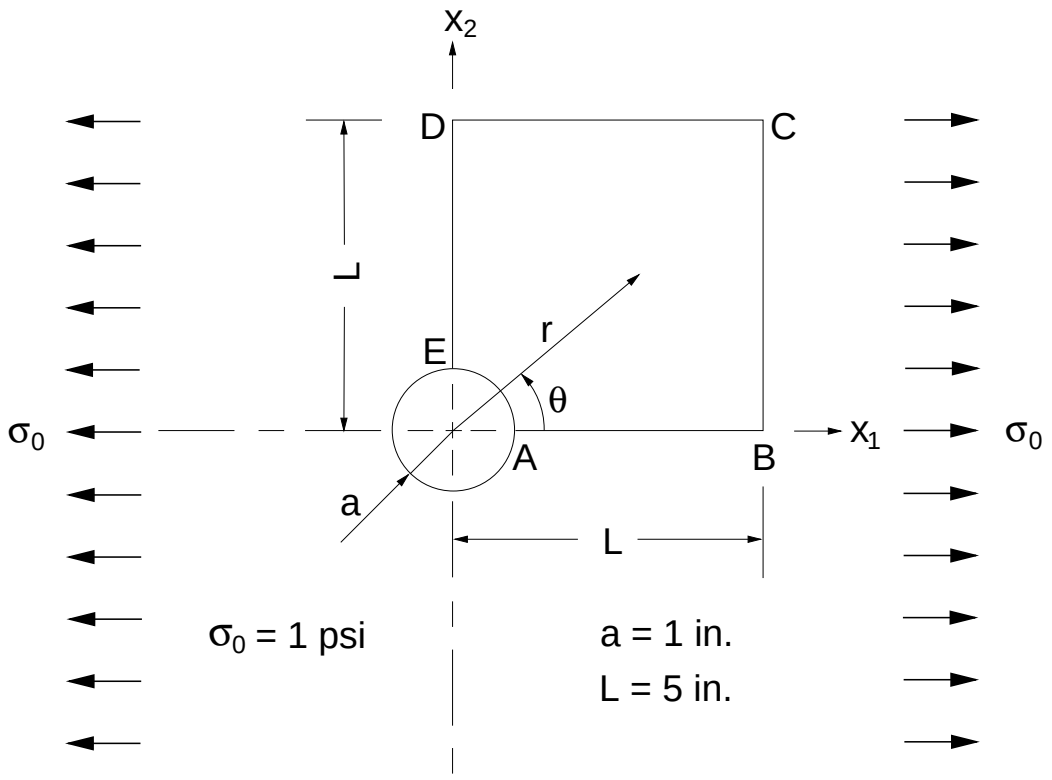

Figure 9: Plate with a circular hole (rigid inclusion) under tension.

which are denoted by R are indicated on the plots. The results indicate that near optimal convergence in displacement and energy is attained for all three values of ν. The absolute accuracy of the C^0–C^{-1} formulation is better than that obtained for the C^0–C^0 formulation; the relative error norms using the mixed C^0–C^{-1} method are independent of the Poisson's ratio ν.

4.3 Rigid Circular Inclusion in an Infinite Plate

As a second benchmark for curvilinear domains, we consider the problem of a rigid circular inclusion in an infinite plate under unidirectional tension (Fig. 9). This problem for the near incompressible case has been studied by many researchers (Szabó, Babauška, and Chayapathy, 1989; Szabó and Babuška, 1991; Chilton and Suri, 1997). Plane strain conditions are assumed in the analysis. The exact displacement components in polar coordinates (r, θ) are (Muskhelishvili, 1953):

$$u_r(r,\theta) = \frac{\sigma_0}{8\mu r}\left\{(\kappa-1)r^2 + 2\gamma a^2 + \left[\beta(\kappa+1)a^2 + 2r^2 + \frac{2\delta a^4}{r^2}\right]\cos 2\theta\right\}, \tag{4.9a}$$

$$u_\theta(r,\theta) = -\frac{\sigma_0}{8\mu r}\left[\beta(\kappa-1)a^2 + 2r^2 - \frac{2\delta a^4}{r^2}\right]\sin 2\theta, \tag{4.9b}$$

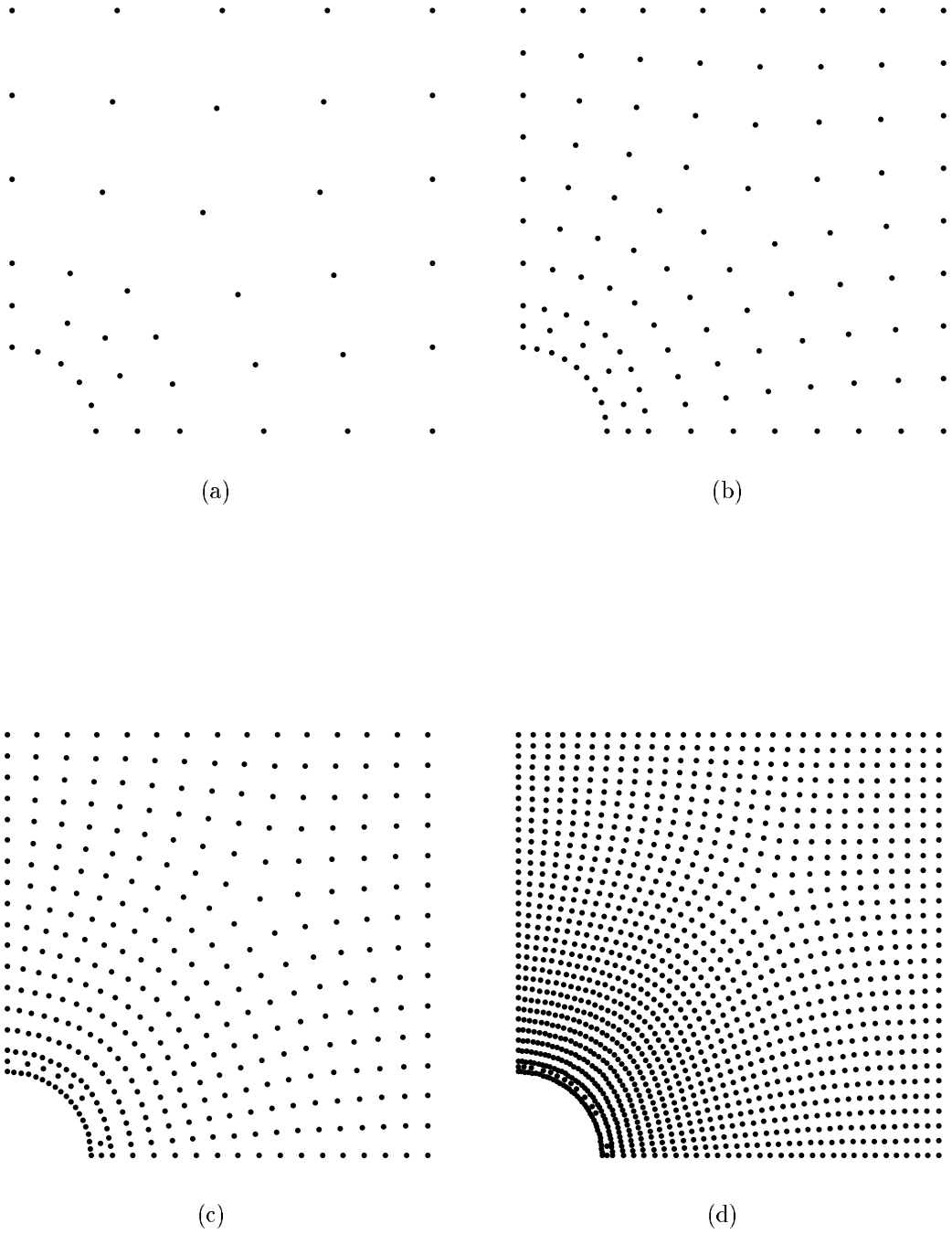

Figure 10: Nodal discretization for the plate with a hole problem. (a) 41 nodes, (b) 108 nodes, (c) 361 nodes, and (d) 1345 nodes.

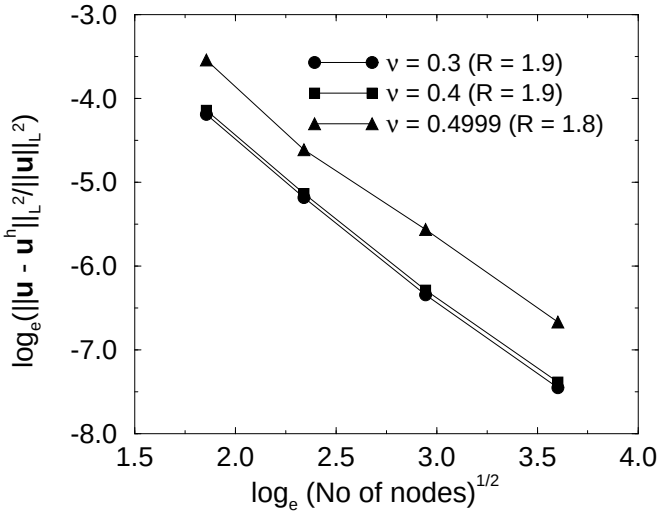

(a)

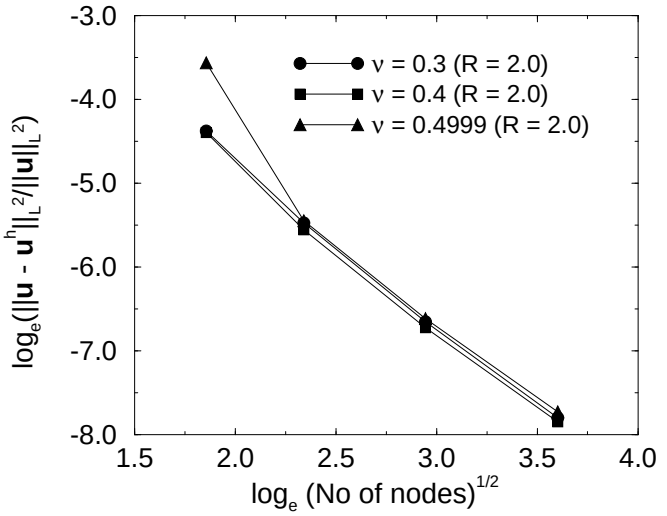

(b)

Figure 11: Rate of convergence in displacement for the plate with a hole problem. (a) C^0–C^0 method, and (b) C^0–C^{-1} method.

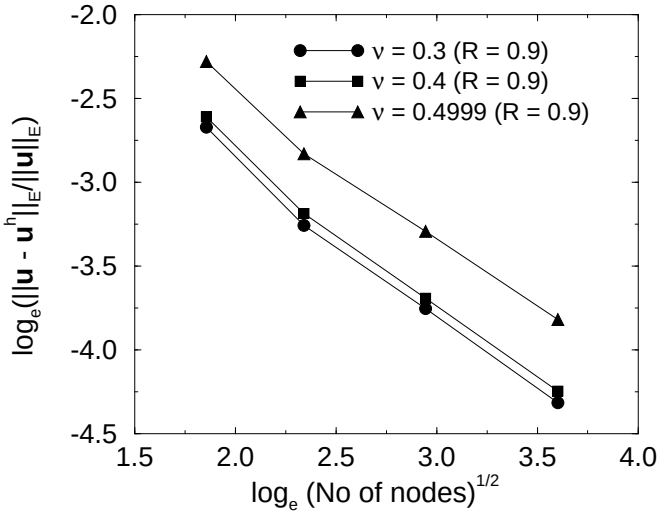

(a)

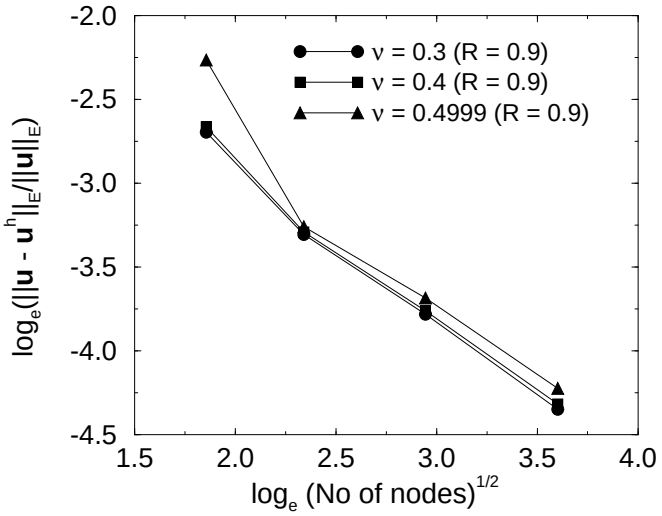

(b)

Figure 12: Rate of convergence in energy for the plate with a hole problem. (a) C^0–C^0 method, and (b) C^0–C^{-1} method.

where μ is the shear modulus, a is the radius of the rigid inclusion, and σ_0 is the applied uniaxial far-field stress. The exact stress components are given by

$$\sigma_r(r,\theta) = \frac{\sigma_0}{2}\left[1 - \frac{\gamma a^2}{r^2} + \left(1 - \frac{2\beta a^2}{r^2} - \frac{3\delta a^4}{r^4}\right)\cos 2\theta\right], \tag{4.10a}$$

$$\sigma_\theta(r,\theta) = \frac{\sigma_0}{2}\left[1 + \frac{\gamma a^2}{r^2} - \left(1 - \frac{3\delta a^4}{r^4}\right)\cos 2\theta\right], \tag{4.10b}$$

$$\sigma_{r\theta}(r,\theta) = -\frac{\sigma_0}{2}\left(1 + \frac{\beta a^2}{r^2} + \frac{3\delta a^4}{r^4}\right)\sin 2\theta. \tag{4.10c}$$

In Eqs. (4.9) and (4.10), κ, β, γ, δ are constants that depend on the Poisson's ratio ν only. For the plane strain case,

$$\kappa = 3 - 4\nu, \quad \beta = -\frac{2}{3-4\nu}, \quad \gamma = -\frac{2-4\nu}{2}, \quad \delta = \frac{1}{3-4\nu}. \tag{4.11}$$

In the numerical computations, $\sigma_0 = 1$ psi, $a = 1$ in., $L = 5$ in., and the nodal grids used are the same as that for the plate with a circular hole problem (see Section 4.2). The notable differences between the two problems lie in the imposition of boundary conditions. Referring to Fig. 9, in order to model the rigid inclusion, the displacement components along the boundary AE are set to zero. Exact tractions are imposed along BC and CD and symmetry displacement boundary conditions are used along AB and DE. The mixed natural element displacement-pressure formulation is applied for the near incompressible case ($\nu = 0.4999$). A convergence study is carried out using the four nodal discretizations shown in Fig. 10, with the $L^2(\Omega)$ and energy error norms used in the computations defined in Eq. (4.4). In Fig. 13, the relative displacement and energy error norms are plotted against the square root of the number of nodes on a log-log plot. Results are presented for the mixed C^0–C^0 displacement-pressure and C^0–C^{-1} displacement-pressure formulations. The convergence rates which are denoted by R are indicated on the plots. Near optimal convergence in displacements and energy is attained for the near incompressible case, with the results for the C^0–C^{-1} formulation being more accurate than those for the C^0–C^0 formulation.

4.4 Pressure Approximation

In order to analyze mixed formulations for validity in the incompressible limit, apart from the rate of convergence in displacement and energy, a pertinent and important notion is the convergence and approximation of the pressure. In mixed finite element methods, the stability (instability) of the approximation spaces is associated with the non-locking (locking) in the numerical solution. The spurious pressure modes points to the solvability of the system which is a consequence of choosing certain approximation spaces in conjunction with certain boundary conditions. For the purpose of analysis, the near incompressible elasticity ($\nu \to 0.5$) problem is equivalent to the

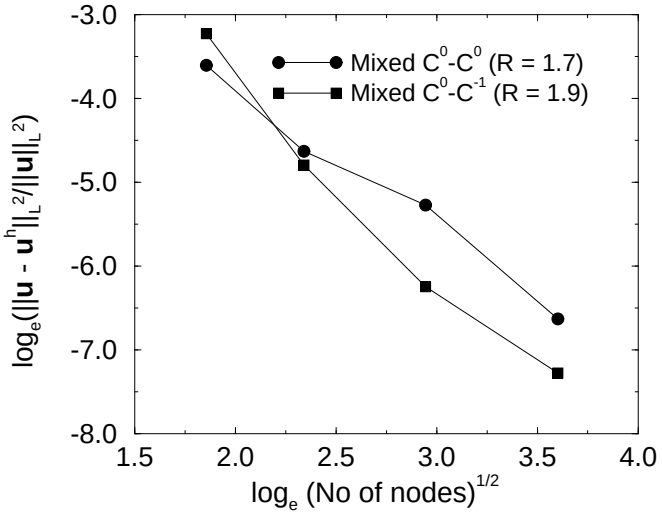

(a)

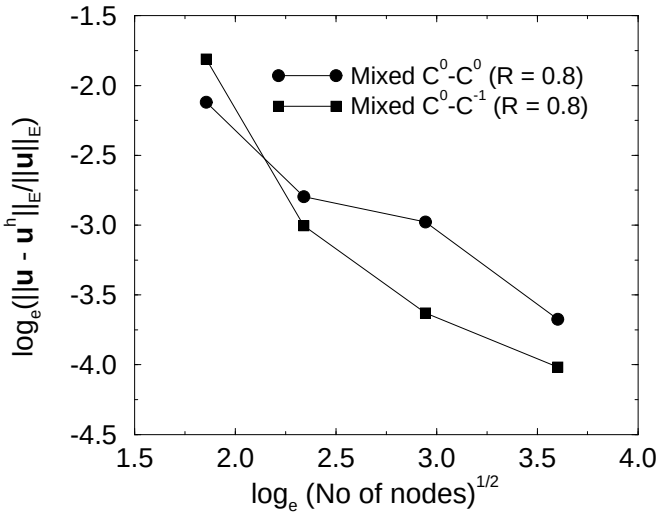

(b)

Figure 13: Rate of convergence in displacement and energy for the rigid inclusion in a plate problem. (a) Displacement, and (b) Energy.

fully incompressible (Stokes) problem. Using $\nu = 0.5$ in Eq. (3.5b), we obtain

$$b(\mathbf{v}^h, p^h) = \int_{\Omega^h} p^h \text{div } \mathbf{v}^h = 0 \quad \forall\, v^h \in V_0^h. \tag{4.12}$$

A non-zero pressure p^h that satisfies the above equation is termed a pressure mode. For purely displacement boundary conditions, a constant pressure p^h is obtained which is a realistic solution. All other pressure solutions to the above equation are known as spurious pressure modes. Pressure filtering (Sani, Gresho, Lee, and Griffiths, 1981; Sani, Gresho, Lee, Griffiths, and Engelman, 1981), least-squares stabilization (Franca and Hughes, 1988), and preconditioning (Pavarino and Widlund, 1997) are some of the means to recover the pollution-free pressure approximation and to enhance stability. Unlike mixed finite element methods, in mixed formulation based on meshless Galerkin methods, the diffuse-character of the approximation renders it difficult to readily observe the presence of spurious pressure modes in numerical simulations. Nonetheless, the pressure approximation and its rate of convergence are useful measures that are readily computed, and which point to the stability of the mixed formulation.

Convergence in the pressure is studied for the mixed NEM formulations. The $L^2(\Omega)$ pressure error norm is defined as:

$$\|p - p^h\|_{L^2(\Omega)} = \Big((p - p^h, p - p^h) \Big)^{1/2}. \tag{4.13}$$

A convergence study is carried out for the three problems discussed in the previous sections. The results of the study are shown in Fig. 14. Clearly, the mixed C^0–C^0 NEM formulation approximates the pressure very poorly. The convergence rate of the mixed C^0–C^{-1} formulation is optimal for the cantilever beam problem (regular discretization), but the convergence rate deteriorates for the plate with the hole and the rigid inclusion problems. As mentioned in an earlier NEM study (Sukumar et al., 1998), inaccuracies in the numerical integration of the weak form do exist in the natural element method. This is primarily due to two factors, namely, the fact that the support of the shape functions do not coincide with the Delaunay triangles used in the numerical quadrature scheme, and secondly the integrands in the weak form are rational functions of spatial coordinates which are not accurately integrated using polynomial-precision symmetric quadrature rules over triangles. With irregular nodal discretization, and in light of the C^{-1} pressure field chosen, numerical integration errors are deemed to be of some significance. However, the sub-optimal rate of convergence in pressure does point to locking in the pressure. Modifications to Galerkin methods, such as least-squares stabilization (Franca and Hughes, 1988) in which residual terms are added to the energy functional, are possible means to enhance stability in the mixed NEM formulation.

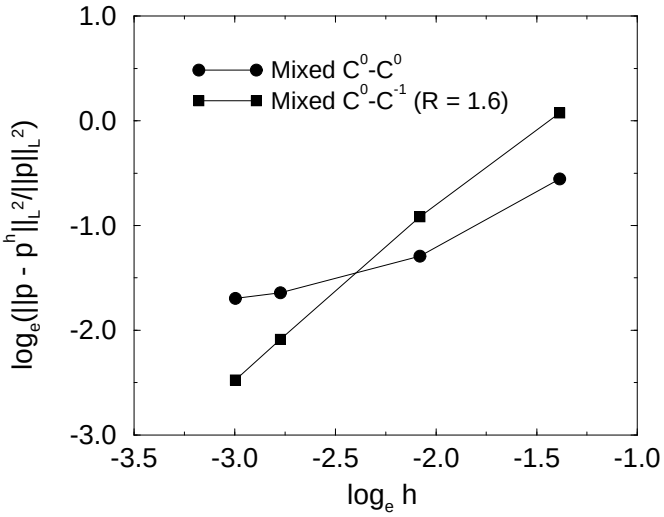

(a)

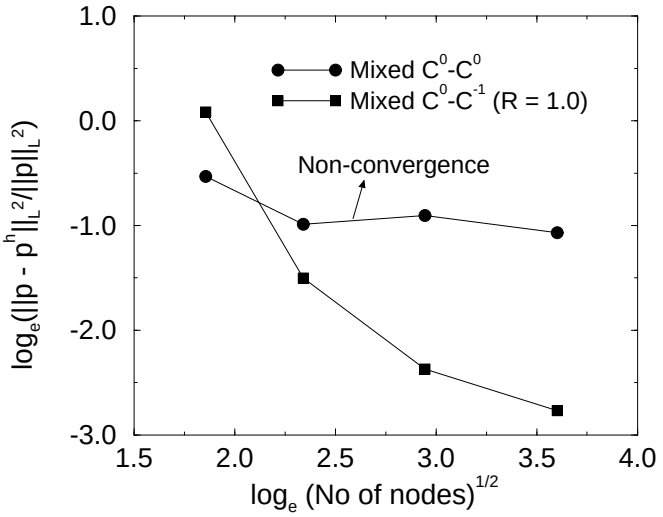

(b)

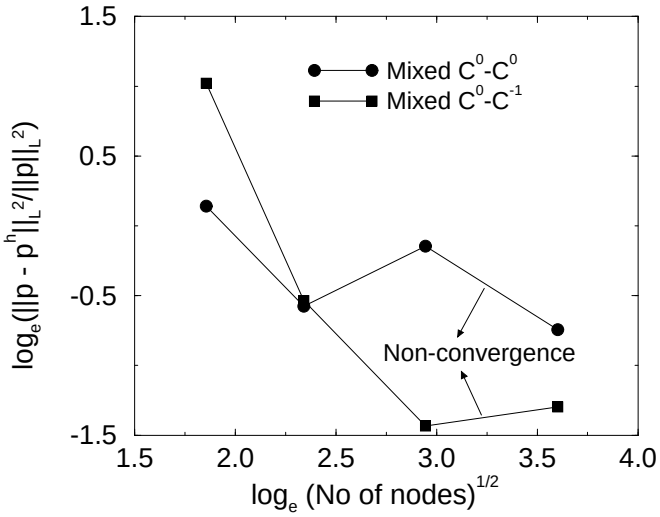

(c)

Figure 14: Convergence of pressure for three benchmark problems. (a) Cantilever beam, (b) Plate with a hole, (c) Rigid inclusion in a plate.

5 Conclusions

Natural neighbor coordinates were proposed by Sibson (1980) as a means for data interpolation and smoothing. In Sukumar et al. (1998) and Sukumar and Moran (1999), its potential as a paradigm for the numerical solution of second-order and fourth-order elliptic PDEs, respectively, was demonstrated. Natural neighbor coordinates have optimum spatial adjacency, and yield a linearly complete approximation. In this paper, a mixed formulation for the natural element method in linear elastostatics was presented. A displacement-pressure mixed formulation was adopted with displacements interpolated by C^0 natural neighbor interpolants; C^0 and C^{-1} interpolation schemes were considered for the interpolation of the pressure field. Numerical results for the beam in bending, plate with a circular hole in tension, and for a rigid inclusion in a plate under uniaxial tension were obtained. The mixed C^0–C^{-1} formulation removed volumetric locking in the near incompressible limit ($\nu \to 0.5$), with optimal convergence rates in displacement and energy for all $\nu \in [0, 0.5)$. For the mixed C^0–C^{-1} formulation, the rate of convergence in the pressure, however, was sub-optimal. It is envisaged that remedies such as pressure projection or least-squares stabilization could lead to stable mixed NEM formulations with accurate pressure approximation and optimal convergence rate in the pressure.

Acknowledgments

The research support of NSF grant CMS–9732319 to Northwestern University is gratefully acknowledged.

References

Arnold, D. N. (1990). Mixed finite element methods for elliptic problems. *Computer Methods in Applied Mechanics and Engineering 82*, 281–300.

Babuška, I. (1971). Error bounds for finite element method. *Numer. Math. 16*, 322–333.

Babuška, I. and M. Suri (1992). Locking effects in the finite element aproximation of elasticity problems. *Numer. Math. 62*, 439–463.

Babuška, I. and Z. Zhang (1998). The partition of unity method for the elastically supported beam. *Computer Methods in Applied Mechanics and Engineering 152*, 1–18.

Belytschko, T., Y. Krongauz, D. Organ, M. Fleming, and P. Krysl (1996). Meshless methods: An overview and recent developments. *Computer Methods in Applied Mechanics and Engineering 139*, 3–47.

Braun, J. and M. Sambridge (1995). A numerical method for solving partial differential equations on highly irregular evolving grids. *Nature 376*, 655–660.

Brezzi, F. (1974). On the existence, uniqueness and approximation of saddle-point problems arising from Lagrange multipliers. *RAIRO Anal. Numér. 8*, 129–151.

Brezzi, F. and M. Fortin (1991). *Mixed and Hybrid Finite Element Methods*. New York: Springer-Verlag.

Chilton, L. and M. Suri (1997). On the selection of a locking-free *hp* element for elasticity problems. *International Journal for Numerical Methods in Engineering 40*, 2045–2062.

Donning, B. (1997). Meshless methods for shear-deformable beams and plates. Master's thesis, Northwestern University.

Dunavant, D. A. (1985). High degree efficient symmetrical Gaussian quadrature rules for the triangle. *International Journal for Numerical Methods in Engineering 21*, 1129–1148.

Farin, G. (1990). Surfaces over Dirichlet tessellations. *Computer Aided Geometric Design 7*(1–4), 281–292.

Franca, L. P. and T. J. R. Hughes (1988). Two classes of mixed finite element methods. *Computer Methods in Applied Mechanics and Engineering 69*, 89–129.

Hermann, L. R. (1965). Elasticity equations for incompressible and nearly incompressible materials by a variational theorem. *AIAA Journal 3*, 1896–1900.

Hughes, T. J. R. (1987). *The Finite Element Method*. Englewood Cliffs, N.J.: Prentice-Hall.

Ladyzhenskaya, O.-A. (1969). *The Mathematical Theory of Viscous Flow* (Second ed.). New York: Gordon and Breach.

Malkus, D. S. and T. J. R. Hughes (1978). Mixed finite element methods—reduced and selective integration techniques: A unification of concepts. *Computer Methods in Applied Mechanics and Engineering 15*, 63–81.

Melenk, J. M. and I. Babuška (1996). The partition of unity finite element method: Basic theory and applications. *Computer Methods in Applied Mechanics and Engineering 139*, 289–314.

Muskhelishvili, N. I. (1953). *Some Basic Problems of the Mathematical Theory of Elasticity* (Third ed.). Groningen, Holland: P. Noordhoff Ltd.

Pavarino, L. F. and O. B. Widlund (1997, December). Iterative substructuring methods for spectral element discretizations of elliptic systems. II: Mixed methods for linear elasticity and Stokes flow. Technical Report 755, Department of Computer Science, Courant Institute of Mathematical Sciences, New York University.

Pian, T. H. H. and K. Sumihara (1984). Rational approach for assumed stress elements. *International Journal for Numerical Methods in Engineering 22*, 173–181.

Preparata, F. and M. Shamos (1985). *Computational Geometry: An Introduction*. New York, N.Y.: Springer-Verlag.

Sani, R. L., P. M. Gresho, R. L. Lee, and D. F. Griffiths (1981). The cause and cure (?) of the spurious pressures generated by certain FEM solutions of the incompressible Navier-Stokes equations: Part I. *International Journal for Numerical Methods in Fluids 1*, 17–43.

Sani, R. L., P. M. Gresho, R. L. Lee, D. F. Griffiths, and M. Engelman (1981). The cause and cure (?) of the spurious pressures generated by certain FEM solutions of the incompressible Navier-Stokes equations: Part II. *International Journal for Numerical Methods in Fluids 1*, 171–204.

Sibson, R. (1980). A vector identity for the Dirichlet tesselation. *Mathematical Proceedings of the Cambridge Philosophical Society 87*, 151–155.

Sibson, R. (1981). A brief description of natural neighbor interpolation. In V. Barnett (Ed.), *Interpreting Multivariate Data*, Chichester, pp. 21–36. John Wiley.

Simo, J. C. and T. J. R. Hughes (1986). On the variational foundations of assumed strain methods. *Journal of Applied Mechanics 53*(1), 51–54.

Sukumar, N. (1998, June). *The Natural Element Method in Solid Mechanics*. Ph.D. thesis, Theoretical and Applied Mechanics, Northwestern University, Evanston, IL, U.S.A.

Sukumar, N. and B. Moran (1999). C^1 natural neighbor interpolant for partial differential equations. *Numerical Methods for Partial Differential Equations 15*(4), 417–447.

Sukumar, N., B. Moran, and T. Belytschko (1998). The natural element method in solid mechanics. *International Journal for Numerical Methods in Engineering 43*(5), 839–887.

Suri, M. (1996). Analytical and computational assessment of locking in the *hp* finite element method. *Computer Methods in Applied Mechanics and Engineering 133*, 347–371.

Szabó, B. and I. Babuška (1991). *Finite Element Analysis*. New York: John Wiley and Sons.

Szabó, B. A., I. Babauška, and B. K. Chayapathy (1989). Stress computations for nearly incompressible materials by the *p*-version of the finite element method. *International Journal for Numerical Methods in Engineering 28*, 2175–2190.

Timoshenko, S. P. and J. N. Goodier (1970). *Theory of Elasticity* (Third ed.). New York: McGraw Hill.

Washizu, K. (1982). *Variational methods in elasticity and plasticity* (Third ed.). Oxford: Pergamon Press.

Watson, D. F. (1992). *Contouring: A Guide to the Analysis and Display of Spatial Data*. Oxford: Pergamon Press.